Journal of Thermal Analysis and Calorimetry (2020) 139:67–73
https://doi.org/10.1007/s10973-019-08368-5

Kinetic study of carbothermal reduction of zirconia under vacuum condition

Faramarz Kazemi[1,2] · Farzin Arianpour[3] · Hamid Reza Rezaie[4]

Received: 1 August 2018 / Accepted: 8 May 2019 / Published online: 29 May 2019

Abstract

In this research, formation mechanism and kinetics of vacuum carbothermal synthesis of zirconium carbide using zirconium acetate and sucrose are discussed. The study of non-isothermal reduction was conducted by thermogravimetry analysis and heating the samples in argon and vacuum conditions up to 1773 K, and then the heat exchange values of reactions were calculated. Isothermal formation mechanism of carbide phase was investigated by heating the samples at 1473 K and 1673 K in argon and vacuum atmospheres followed by X-ray diffraction and quantitative phase analysis. Results showed that in non-isothermal state, the carbothermal reduction of zirconia is a heterogeneous reaction with multiple steps. For isothermal reaction, the kinetic parameters such as activation energy and pre-exponential factor were calculated as 70.56 kJ mol^{-1} and 11.22×10^{-2} S^{-1}, respectively. It was presented that the activation energy value extracted from isothermal reaction is completely in accordance with the final step of non-isothermal results.

Keywords Zirconium carbide · Vacuum · Carbothermal reduction · Thermal analysis · Kinetics

List of symbols

R	Gas constant (8.314 J mol^{-1} K^{-1})
α	Extent of reaction
m_0	Initial sample mass (g)
m_T	Final sample mass (g)
m_{ZrO_2}	123.218 g mol^{-1}
A	Pre-exponential factor (S^{-1})
E	Activation energy
$\ln\left(\frac{g(\alpha)}{T^2}\right)$	Effective rate constant
I	Peak intensity
I_n	Peak intensity in nth step
$h(p)$	Pressure dependence function
P_{eq}	Equilibrium vapor pressure
m_c	12.01 g mol^{-1}
α'	$\frac{d\alpha}{dT}$
T	Temperature (K)
$f(\alpha)$	Differential reaction model contracting sphere: $3(1-\alpha)^{2/3}$
$g(\alpha)$	Integral reaction model contracting sphere: $1-(1-\alpha)^{1/3}$
β	Heating rate (10 K min^{-1})
t	Time (s)
$2\theta_o$	Initial 2θ of (002) ZrC peak
$2\theta_f$	Final 2θ of (002) ZrC peak
I_n^0	Background intensity of peak in nth step
b	Constant value between 0.5 and 1.5
P_{CO}	Partial pressure of $CO_{(g)}$

✉ Hamid Reza Rezaie
hrezaie@iust.ac.ir

[1] Department of Mining and Metallurgy, Amirkabir University of Technology, Tehran, Iran

[2] Kimia Zanjan Gostaran Co., Zanjan, Iran

[3] Research and Application Center, Kastamonu University, Kastamonu, Turkey

[4] School of Metallurgy and Materials Engineering, Iran University of Science and Technology, Tehran, Iran

Introduction

Zirconium carbide (ZrC) is a kind of ultra-high-temperature ceramics (UHTCs) which shows excellent properties such as high melting point, considerable wear resistance, high-temperature structural stability, high strength and hardness [1]. Thanks to mentioned properties, this material has a wide range of applications such as mechanical parts, cutting tools and in other high-tech industries regarding its superior physical and mechanical properties, especially its low-density value in comparison with other UHT carbide materials [1, 2]. Various methods have been developed to

produce ZrC powder including carbothermal synthesis [3–5], combustion synthesis [6–8], self-propagating high-temperature synthesis [9], laser pyrolysis [10], magnesiothermic [11] and spark plasma sintering [12]. In most of these techniques, the carbothermal reduction of zirconia is the main formation mechanism of ZrC.

There are some reports on the formation kinetics study of transition metal carbide such as titanium carbide (TiC) [13–15], manganese carbide (Mn_7C_3) [16], nickel carbide (Ni_3C) [17] and tungsten carbide (WC) [18, 19]. Thermogravimetric analysis (TG) followed by X-ray diffraction (XRD) is one of the practical methods for kinetic study of carbothermal reduction synthesis of carbide materials [14, 20]. Kahrizsangi et al. [21] investigated the non-isothermal kinetic of carbothermal reduction of submicron zirconia and graphite under argon flow via thermogravimetric analysis. Activation energy of carbothermal reduction was calculated to be equal to 273 kJ mol^{-1} via Coats-Redfern method which was very similar to the results obtained by Maitre et al. [22]. The evaluation of reaction extent between carbon black and micron-size zirconia under argon flow was performed by calculating mass loss at different temperatures and heat treatment durations [23]. The results of these researches showed that the reaction occurs in homogeneous condition regarding linear plot of the effective rate, i.e., $\ln\left(\frac{g(\alpha)}{T^2}\right)$ against $\frac{1}{T}$ [24]. David et al. [25] stated that the reaction between submicron zirconia powder and nano-sized carbon black happens in multiple steps which is associated with zirconium carbide condensation from gas-phase reaction of CO and ZrO.

In the current research, carbothermal reduction of zirconia under argon flow and vacuum condition was investigated via thermogravimetric analysis (TG) and X-ray diffraction (XRD). The activation energy of carbide phase formation in non-isothermal reaction was driven out from TG data. In addition, isothermal reaction parameters for vacuum atmosphere were calculated from quantitative X-ray analysis. Results show the activation energy of carbothermal reduction under vacuum atmosphere was less than same reduction in argon flow.

Experimental

Zirconium acetate (22 mass/% aq. solution, Astron Chemicals, Australia), sucrose (Merck, Germany) and polyvinyl alcohol (Merck, Germany) were used as starting materials in this work. The molar ratio of sucrose to zirconium acetate and polyvinyl alcohol (PVA) was set to 0.25:1:0.0312. The carbon to zirconium ion molar ratio was adjusted to 3 according to stoichiometric reduction of zirconia. All starting materials were dissolved into deionized water, and pH was set to 1 by dropwise addition of diluted nitric acid and then mixing continued until a viscose brown gel was made. The gel was dried in an electric oven at 473 K for 4 h and then fine-milled using agate mortar. The final product was then passed through − 75-μm sieve to obtain homogenous powder and break any possible large agglomerates. The formation temperature of ZrC from dried gel was followed by thermogravimetric analysis (TG) in argon and vacuum conditions. Thermal analysis was done up to 1773 K using a simultaneous thermal analyzer (STA 503, BAHR, Germany) system with a heating rate of 10 K min^{-1} using alumina crucibles in argon (10 mL min^{-1} flow rate) and vacuum (10^{-6} mbar) conditions, separately. For isothermal study, powdered samples were poured into the alumina crucibles and calcined in a tube furnace by heating rate of 10 K min^{-1} at 1473 K (3 h) and 1673 K (3 h) in argon flow (20 mL min^{-1} flow rate) and 1473 K (1, 3, 5 and 7 h) and 1673 K (3 h) in vacuum condition (10^{-6} mbar). After firing, the products were fine-milled using agate mortar to produce homogenous powders and then investigated by X-ray diffraction (XRD, Cu Kα 30 mA 40 kV, PW1800 Philips, Netherland). Figure 1 shows the schematic details of nano-ZrC powder synthesis and experimental procedure.

Results and discussion

Figure 2 shows the recorded TG curves of the dried gel powder after heating up to 1500 °C in argon and vacuum conditions separately. Regarding mass loss during TG analysis, it is clear that the carbothermal reduction starts after sample mass reaches 18.73 mg. In addition, the final mass of the sample heated under vacuum was about 10 mass/% lower than the sample heated in argon flow. It is found that the decreases in the O_{2g} and CO_g partial pressures during the formation of ZrC via carbothermal reduction would be very effective to reduce 423–473 K of synthesis temperature [25–27]. As Fig. 2 shows, the formation temperature of carbide phase could dramatically decrease under vacuum condition. This phenomenon can be described by reaction Eq. (1):

$$ZrO_2 + 3C \rightarrow ZrC + 2CO \quad \Delta G = \Delta G^{o} + 2RTLnP_{co} \tag{1}$$

The extent of reaction (α) is calculated according to Eq. (2) [27, 28] and the variation of α factor against temperature after starting the reaction for vacuum- and argon-heated samples presented in Fig. 3. As it is illustrated, α factor for argon-heated sample was brought to 0.8 while for vacuum-heated one it reached 1 showing completion of reduction process.

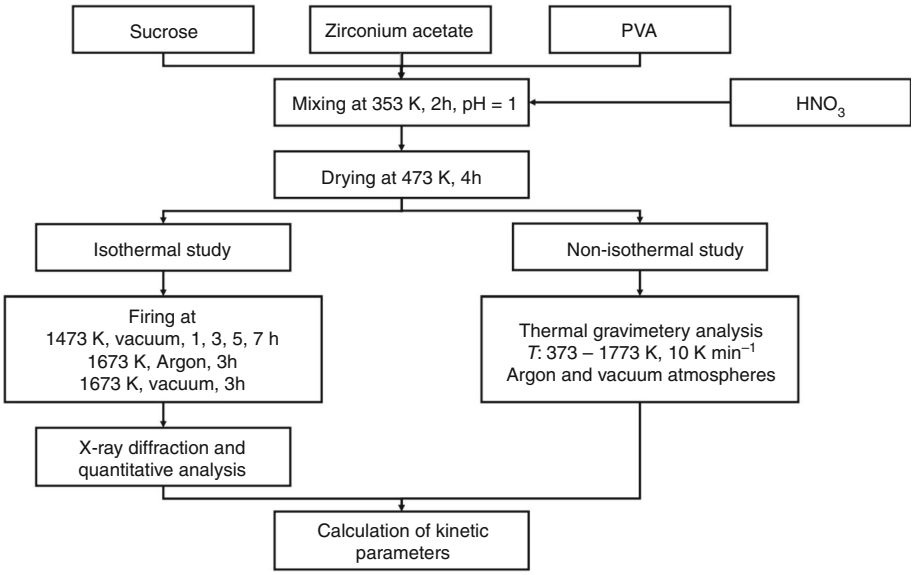

Fig. 1 Schematic of samples preparation and experimental procedure

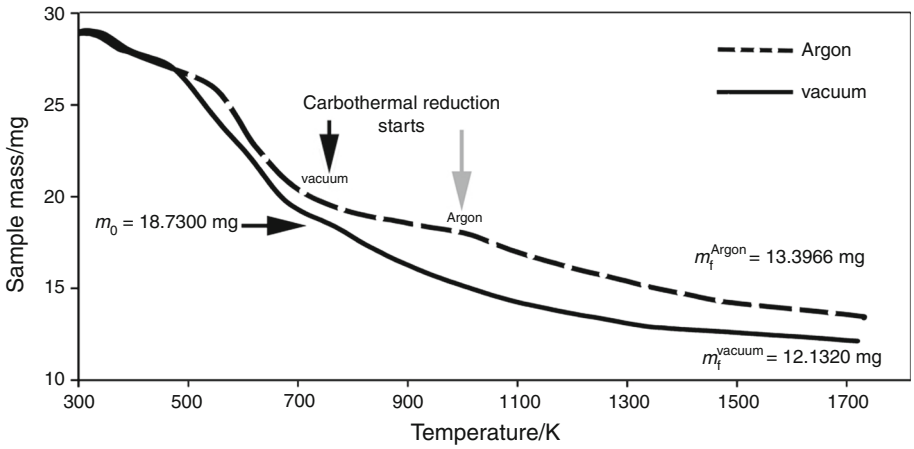

Fig. 2 Thermogravimetric (TG) analysis of precursors heated in argon and vacuum

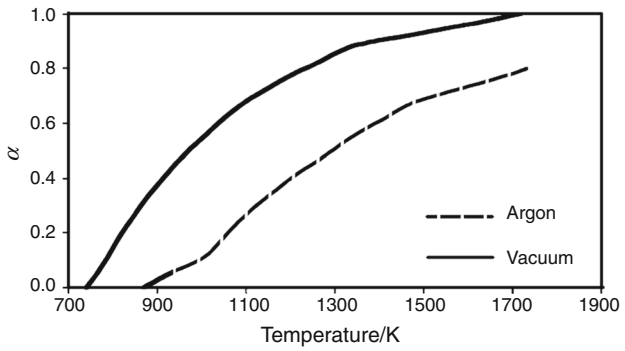

Fig. 3 Extent of carbothermal reaction (α) versus temperature in argon and vacuum

$$\alpha = \frac{m_o - m_T}{m_o - x m_o}, \quad x = \frac{(m_{ZrO_2} + 3m_C) - m_{ZrC}}{m_{ZrO_2} + 3m_C} = 0.352201 \tag{2}$$

In case of non-isothermal reaction, the activation energy can be calculated by Eqs. (3), (4) and (5) [29, 30]:

$$\frac{d\alpha}{dT} = \frac{A}{\beta}\exp\left(\frac{-E}{RT}\right) f(\alpha), \tag{3}$$

$$\ln \alpha' - ln(f(\alpha)) = \ln\frac{A}{\beta} - \frac{E}{RT} \tag{4}$$

$$\frac{d\left(\ln\frac{\alpha'}{f(\alpha)}\right)}{d\left(\frac{1}{T}\right)} = -\frac{E}{R} \tag{5}$$

In addition, there are some other methods for calculating activation energy by non-isothermal thermogravimetry according to Eq. (6) [31–33]:

$$\ln\left(\frac{g(\alpha)}{T^2}\right) = \ln\left[\frac{AR}{\beta E_a}\left(1 - \frac{2R\bar{T}}{E_a}\right)\right] - \frac{E_a}{RT} \tag{6}$$

Figure 4 is drawn by plotting the calculated activation energy data (obtained from TG analysis) against

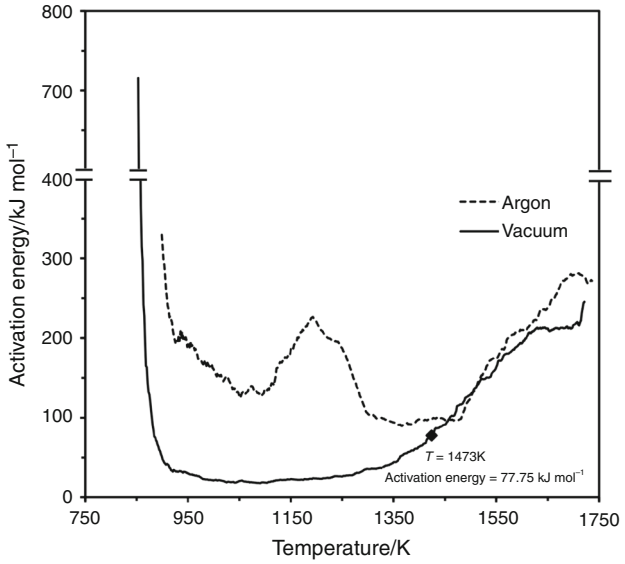

Fig. 4 Activation energy values versus temperature in non-isothermal formation of ZrC in vacuum and argon

temperature using the first method based on Eqs. (3)–(5). As this figure shows, the activation energy was not constant during carbothermal reduction which confirms the presence of multiple steps and reactions. Kahrizsangi et al. [21] and Maitre et al. [22] plotted the curve of $\ln\left(\frac{g(\alpha)}{T^2}\right)$ term, i.e., x effective rate constant versus $\frac{1}{T}$, and fitted a linear function in their works. In their researches, the activation energy of the reaction is identified by the line's slope as $\frac{E_a}{R}$ .They reported the calculated activation energy of the carbothermal reduction reaction in argon flow is equal to 273 kJ and 219 kJ. In the both studies, the activation energy was determined independently from the extent of reaction according to constant value of activation energy versus temperature [27]. David et al. [25] used submicron zirconia and nano-sized carbon black as precursors and prepared samples by heat-treating under argon. It is proposed that, at the first step, zirconia could be reduced and evaporated as ZrO gas phase (Eq. 7), and then by reacting with CO_g (Eq. 5), oxy-carbide phase can be condensed in the second step according to Eq. (9). Finally, in the last step, oxy-carbide phase can be reduced by CO_g to form ZrC phase (Eq. 10):

$$ZrO_{2(s)} \rightarrow ZrO_{(g)} + \frac{1}{2}O_{2(g)} \tag{7}$$

$$C_{(s)} + CO_{2(g)} \rightarrow 2CO_{(g)} \tag{8}$$

$$ZrO_{(g)} + (3-3\delta)CO_{(s)} \rightarrow ZrO_{\delta}C_{(1-\delta)(s)} + (2-2\delta)CO_{2(g)} \tag{9}$$

$$ZrO_{\delta}C_{(1-\delta)(s)} + 3\delta CO_{(g)} \rightarrow ZrC_{(s)} + 2\delta CO_{2(g)} \tag{10}$$

According to Figs. 2 and 3, the first stage of reaction starts from 720 K which is associated with reaction Eqs. (7) and (8) and ends at 950 K in vacuum condition. In this step, as it can be seen in Fig. 4, the activation energy of these reactions was higher than 500 kJ mol^{-1}. During this step, carbon from sucrose reduces zirconia and then CO and ZrO gases can be formed synchronously in vacuum condition. However, it seems that in argon flow, reduction of ZrO_2 (Eq. 10) and oxidation of carbon (Eq. 8) did not occur synchronously according to the presence of a peak in the curve of Fig. 4. It can be declared that the first step begins from 950 K and ends at about 1320 K which has the maximum activation energy value during carbothermal reaction of zirconia in argon atmosphere. In the second step, which is the chemical reaction between ZrO and CO gas phases, the produced oxy-carbide phase begins to precipitate due to Eq. (9). As it can be seen in Fig. 4, this step starts from 950 to 1350 K for carbothermal reduction in vacuum condition. Finally from 1350 till 1750 K, the activation energy of the reaction in both argon and vacuum conditions increased approximately linearly. However, the activation energy of reaction in vacuum condition was constantly lower than argon flow in all steps. According to the above data, since the activation energy of the reaction is a function of parameters such as extent of reaction (α), temperature and state of the reaction, it can be declared that the carbothermal reduction in both vacuum and argon atmospheres is a heterogeneous reaction [23].

As Figs. 3 and 4 show, the α factor curve versus temperature has a slight slope change according to the final step of zirconium carbide phase formation (Eq. 10) in near 1400 K. Therefore, this temperature was chosen for further investigations on isothermal exercises. For calculating the kinetic parameters of reaction which are pre-exponential factor (A) and activation energy (E), two different temperatures such as 1473 and 1673 K should be investigated as binary condition for Eq. (11). Since the formation of carbide phase nearly comes to an end at 1673 K [26], the latter temperature is selected as secondary condition. Figures 5 and 6 show the X-ray diffraction patterns of samples heated at 1473 K and 1673 K for 3 h in argon and vacuum conditions, respectively. As these figures show, the carbide content of samples heat-treated in vacuum is extraordinarily higher than that the one heated in argon at 1673 K. In order to investigate the isothermal kinetic of carbide phase formation under vacuum condition, some samples were heated at 1473 K for 1, 3, 5 and 7 h of soaking time in vacuum and then analyzed by X-ray diffractometry. Figure 7 shows the obtained X-ray diffraction patterns and the evaluation of carbide phase in these samples. As this figure shows, since there is no evidence of zirconia phase

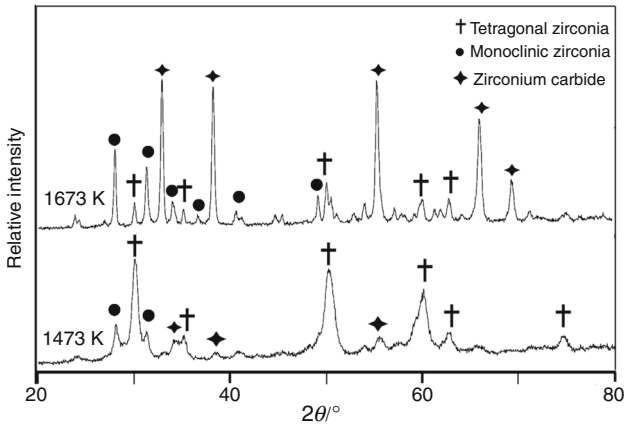

Fig. 5 XRD patterns of samples heated at 1473 and 1673 K for 3 h in argon

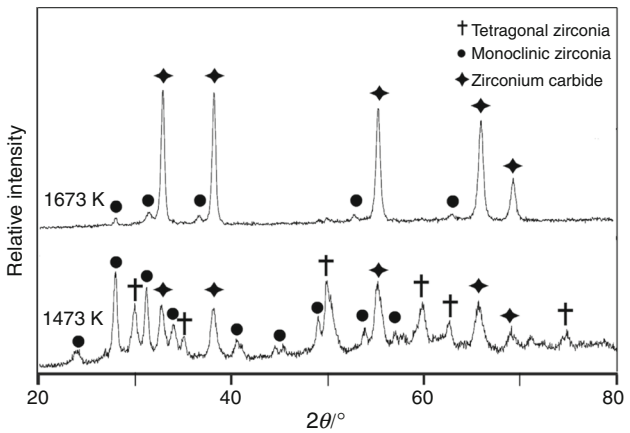

Fig. 6 XRD patterns of samples heated at 1473 and 1673 K for 3 h in vacuum

presence in X-ray diffraction patterns, it can be revealed that the carbothermal reduction of zirconia is completed after 7-h heating under vacuum condition. The amounts of carbide phase were calculated approximately from (111) peak area of ZrC via integration using Eq. (12) [34]. Table 1 lists the calculated area values and the estimated carbide phase content of each sample.

$$t = \frac{g(\alpha)}{A\exp\left(\frac{-E}{RT}\right)},\ \ln(t) = \ln\left(\frac{g(\alpha)}{A}\right) + \frac{E}{RT},\ \ln\left(\frac{g(\alpha)}{A}\right) = \ln(t) - \frac{E}{RT} \tag{11}$$

$$\text{Area} = \int_{2\theta_0}^{2\theta_f} I(2\theta)\mathrm{d}2\theta \cong \sum_{n=0}^{n=f}\left(I_\mathrm{n} - I_\mathrm{n}^0\right)\cdot\Delta 2\theta \tag{12}$$

The activation energy of carbide phase formation in isothermal condition was calculated from Eq. (12) [32]. The average value of $11.22 \times 10^{-2}\ \mathrm{S}^{-1}$ was obtained for

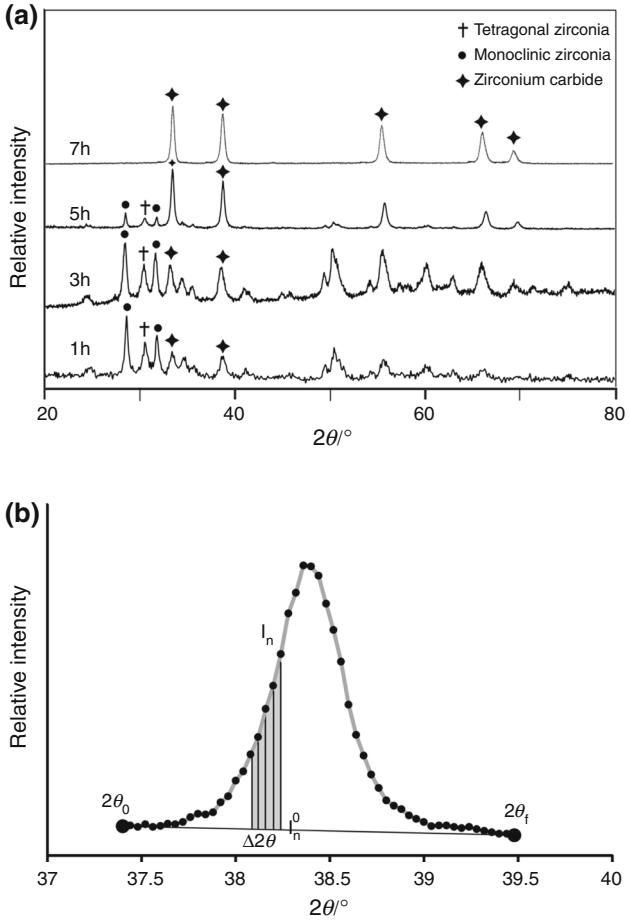

Fig. 7 XRD patterns of samples heated at 1473 K for 1, 3, 5 and 7 h in vacuum (**a**) and schematic of numerical integral of area under the (002) ZrC peak (**b**)

Table 1 Calculated ZrC-phase contents of heated samples in vacuum

Temperature/K	1473	1473	1473	1473	1673
Time/s	3600	10,800	18,000	25,200	10,800
ln(t)	8.1886	9.2873	9.7981	10.1346	9.2873
Area/2θ count	16.51	26.5	35.29	37.18	36.4
Phase content /vol%	29	65	92	97	95
$g(\alpha)$	0.1078	0.2952	0.5703	0.6892	0.6315
$A \times 10^{-2}/\mathrm{S}^{-1}$	8.045	15.81	5.33	15.7	–

pre-exponential factor and used for plotting Fig. 8. By drawing $\ln\left(\frac{g(\alpha)}{A}\right)$ against $\ln(t)$ and fitting a linear function, the activation energy values of carbide phase formation in isothermal condition were derived out from constant term of the linear equation which is $-\frac{E}{RT}$ (Fig. 8). According to these calculations, activation energy of carbothermal reduction at 1473 K was equal to 70.5 kJ mol^{-1}. The calculated parameters and pre-exponential factor of

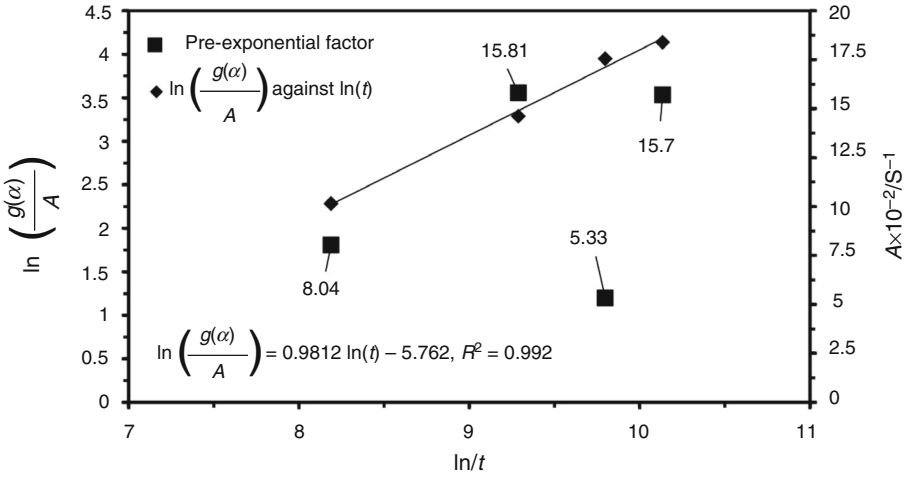

Fig. 8 Activation energy of isothermal zirconia reduction at 1473 K in vacuum

isothermal reaction are presented in Table 1. The estimated isothermal activation energy from the above procedure is approximately close to the calculated activation energy from non-isothermal method which was equal to 77.75 kJ mol^{-1}.

It can be declared that the activation energy of zirconia carbothermal reduction under vacuum condition was decreased in comparison with other researches. Also the obtained pre-exponential factor in this research shows that the total number of atomic collisions per second in vacuum condition is much less than other references such as 10^9 S^{-1} [21] and 25.6 S^{-1} [22]. In the former reference graphite and in latter one, carbon black was used as source of carbon; therefore, the kinetic parameters mentioned in these references are different. For reactions which are pressure dependence, the Arrhenius equation (Eq. 3) could be described as Eq. (13) [35]:

$$\frac{d\alpha}{dt} = k(T)f(\alpha)h(p) \tag{13}$$

$$k(T) = A'T^{b}e^{\frac{-E_a}{RT}}, \quad A'' = A' \cdot T^{b}, A = A'' \cdot h(P), \tag{14}$$

$$h(p) = 1 - \frac{P_{CO}}{P_{eq}}, \quad P_{eq} = 10^{-9} \text{ bar} \tag{15}$$

According to the isothermal condition for carbothermal reduction (Eq. 1), $A' \cdot T^{b}$ term of Eq. (14) could be considered as A''. The thermodynamic equilibrium pressure of CO, CO_2, O_2 and ZrO gases has also been calculated by using HSC software [36] equal to 9.99×10^{-10}, 8.45×10^{-16}, 1.40×10^{-22} and 7.53×10^{-30} bar, respectively, and then $h(p)$ was calculated to be equal to 8.45×10^{-7}. Therefore, the small amount of calculated pre-exponential factor (11.22×10^{-2} S^{-1}) in comparison with other references could be explained due to small amount of $h(p)$ function in vacuum condition.

Conclusions

The kinetics of carbothermal reduction of zirconia after heating at 1473 K and 1673 K in argon and vacuum conditions were investigated and compared via thermogravimetric (TG) and X-ray diffraction (XRD) techniques. The results showed that the initial reduction temperatures of calcined samples in argon and vacuum are 870 K and 740 K, respectively. The extent of reaction (α) factor of non-isothermal reaction reached 0.82 for sample heated in argon flow, while it is demonstrated the reaction could be completed under vacuum condition by the same heating regime. The activation energy values of the carbothermal reduction at different conditions were calculated, and the obtained results presented the possibility of three different steps for zirconia carbothermal reaction. However, the first step of reaction in argon flow was associated with semi-reduction of zirconia and formation of ZrO and CO gas phases at different temperatures, these reactions were performed simultaneously under vacuum condition. Therefore, the activation energy of sample which was heat-treated in argon was much higher than the one heated in vacuum. In the second step, by deposition of oxy-carbide phase from gas-state reaction, the activation energy decreased and in the final step, during deoxygenation of oxy-carbide phase, it increased in both conditions. These obtained results demonstrate that the carbothermal reduction of zirconia is a kind of heterogeneous reaction. Finally, the isothermal reduction was investigated and results showed that the activation energy of reaction at 1473 K is about 70 kJ mol^{-1} which is close to the calculated results of non-isothermal reaction. In addition, the pre-exponential factor of carbothermal reduction under vacuum condition was obtained as 11.2×10^{-2} S^{-1}, and according to thermodynamic calculations, it could be concluded that the reaction is pressure dependent.

References

1. Fahrenholtz WG, Wuchina EJ, Lee WE, Zhou Y. Ultra-high temperature ceramics: materials for extreme environment applications. USA: Wiley; 2014.
2. Arianpour F, Golestanifard F, Rezaie HR, Mazaheri M, Celik A, Kara F, Fantozzi G. Processing, phase evaluation and mechanical properties of $MoSi_2$ doped 4TaC-HfC based UHTCs consolidated by spark plasma sintering. Int J Refract Met Hard Mater. 2016;56:1–7.
3. Dolle M, Gosset D, Bogicevic C, Karolak F, Simeone D, Baldinozzi G. Synthesis of nanosized zirconium carbide by a sol-gel route. J Eur Ceram Soc. 2007;27:2061–7.
4. Stolle S, Gruner W, Pitschke W, Berger LM, Wetzig K. Comparative microscale investigations of the carbothermal synthesis of (Ti, Zr, Si) carbides with oxide intermediates of different volatilities. Int J Refract Met Hard Mater. 2000;18:61–72.
5. Shen G, Chen D, Liu Y, Tang K, Qian Y. Synthesis of ZrC hollow nano spheres at low temperature. J Cryst Growth. 2004;262:277–80.
6. Zhang MX, Hu QD, Huang B, Li JZ, Li JG. Study of formation behavior of ZrC in the Fe–Zr–C system during combustion synthesis. Int J Refract Met Hard Mater. 2011;29:596–600.
7. Zhang MX, Huanga B, Hua QD, Lia JG. Study of formation behavior of ZrC in the Cu–Zr–C system during combustion synthesis. Int J Refract Met Hard Mater. 2012;31:230–5.
8. Hu Q, Zhang M, Luo P, Song M, Li J. Thermal explosion synthesis of ZrC particles and their mechanism of formation from Al–Zr–C elemental powders. Int J Refract Met Hard Mater. 2012;35:251–6.
9. Li J, Fu ZY, Wang WM, Wang H, Lee SH, Niihara K. Preparation of ZrC by self-propagating high-temperature synthesis. Ceram Int. 2010;36:1681–6.
10. Combemale L, Leconte Y, Portier X, Herlin-Boime N, Reynaud C. Synthesis of nano sized zirconium carbide by laser pyrolysis route. J Alloys Compd. 2009;483:468–72.
11. Ji Z, Ye L, Tao X, Li H, Qiu W, Cai T, Jiang Y, Zhao T. Synthesis of ordered mesoporous ZrC/C nanocomposite via magnesiothermic reduction at low temperature. Mater Lett. 2012;71:88–90.
12. Feng L, Lee S, Lee H. Nano-sized zirconium carbide powder: synthesis and densification using a spark plasma sintering apparatus. Int J Refract Met Hard Mater. 2017;64:98–105.
13. Koc R. Kinetics and phase evolution during carbothermal synthesis of titanium carbide from carbon-coated titania powder. J Eur Ceram Soc. 1997;17:1309–15.
14. Koc R. Kinetics and phase evolution during carbothermal synthesis of titanium carbide from ultrafine titania carbon mixture. J Mater Sci. 1998;33:1049–55.
15. Gou H, Zhang G, Hu X, Chou K. Kinetic study on carbothermic reduction of ilmenite with activated carbon. Trans Nonferrous Met Soc China. 2017;27:1856–61.
16. Kim D, Jeong I, Jung S. Kinetic study on carbothermic reduction of MnO_2 with graphite. Ironmaking Steelmaking. 2016;43:526–32.
17. Leng Y, Xiea L, Liaoa F, Zhenga J, Li X. Kinetic and thermodynamics studies on the decompositions of Ni3C in different atmospheres. Thermochim Acta. 2008;473:14–8.
18. Cetinkaya S, Eroglu S. Comparative kinetic and structural analyses of nanocrystalline WC powder synthesis from pre-reduced W under pure and diluted CH_4 atmospheres. Int J Refract Met Hard Mater. 2011;29:214–20.
19. Kharatyan SL, Chatilyan HA, Arakelyan LH. Kinetics of tungsten carbidization under non-isothermal conditions. Mater Res Bull. 2008;43:897–906.
20. Cairo CA, Florian M, Grac ML, Bressiani JC. Kinetic study by TGA of the effect of oxidation inhibitors for carbon–carbon composite. Mater Sci Eng A. 2003;358:298–303.
21. Ebrahimi Kahrizsangi R, Amini Kahrizsangi E. Zirconia carbothermal reduction: non-isothermal kinetics. Int J Refract Met Hard Mater. 2009;27:637–41.
22. Maitre A, Lefort P. Solid state reaction of zirconia with carbon. Solid State Ionics. 1997;104:109–22.
23. Bokstein B. Thermodynamics and kinetics in materials science. Oxford: Oxford University Press; 2005.
24. Deb P. Kinetics of heterogeneous solid state processes. London: Springer; 2014.
25. David J, Trolliard G, Gendre M, Maitre A. TEM study of the reaction mechanisms involved in the carbothermal reduction of zirconia. J Eur Ceram Soc. 2013;33:165–79.
26. Arianpour F, Kazemi F, Rezaie HR, Asjodi A, Liu J. Nano zirconium carbide powder synthesis via carbothermal route. Defect Diffus Forum. 2013;334–335:381–6.
27. Ebrahimi Kahrizsangi R, Abbasi MH. Evaluation of reliability of Coats-Redfern method for kinetic analysis of non-isothermal TGA. Trans Nonferrous Met Soc China. 2008;18:217–21.
28. Jerez A, Ramos E, Gaitan M, Veiga ML, Pico C. A method for the kinetic analysis of non-isothermal decomposition reactions of solids. Thermochim Acta. 1987;115:175–80.
29. Denisov ET, Sarkisov OM, Likhtenshtein GI. Chemical kinetics: fundamentals and new developments. Moscow: Elsevier; 2003.
30. Moser G, Tschamber V, Schonnenbeck C, Brillard A, Brilhac JF. Non-isothermal oxidation and kinetic analysis of pure magnesium powder. J Therm Anal Calorim. 2018. https://doi.org/10.1007/s10973-018-7845-z.
31. Vyazovkin S, Wight CA. Isothermal and non-isothermal kinetics of thermally stimulated reactions of solids. Int Rev Phys Chem. 1998;17:407–33.
32. Vyazovkin S, Wight CA. Model-free and model-fitting approaches to kinetic analysis of isothermal and non-isothermal data. Thermochim Acta. 1999;340–341:53–68.
33. Aboulkas A, El-Harfi K. Study of the kinetics and mechanisms of thermal decomposition of Moroccan Tarfaya oil shale and its kerogen. Oil Shale. 2008;25:426–43.
34. Jenkins R, Snyder RL. Introduction to X-ray powder diffractometry. Hoboken: Wiley; 1996.
35. Burnham AK. Global chemical kinetics of fossil fuels: how to model maturation and pyrolysis. New York: Springer; 2017.
36. HSC Chemistry for Windows-Chemical Reaction and Equilibrium Software, Outokumpu Research Oy, Pori, Finland; 2006.